Motivations, successes, and problems, with the Lagrangian-remap dynamical core in MOM6

Alistair Adcroft

Princeton University / NOAA-GFDL

Z-coordinates v. isopycnal coordinates

- Winton et al., 1998: z-coordinate models excess mixing in overflows
  - Numerous coordinate/mixing studies: Griffies et al., 2000; Chassignet et al., 2003; Legg et al., 2006; Burchard & Rennau 2008; Megann et al., 2010; …
- Dunne et al., 2012: compared ESM2M and ESM2G, both 1° resolution
  - ESM2M: z-coordinate, shallow AMOC
  - ESM2G: isopycnal layer model, deep AMOC with overflows

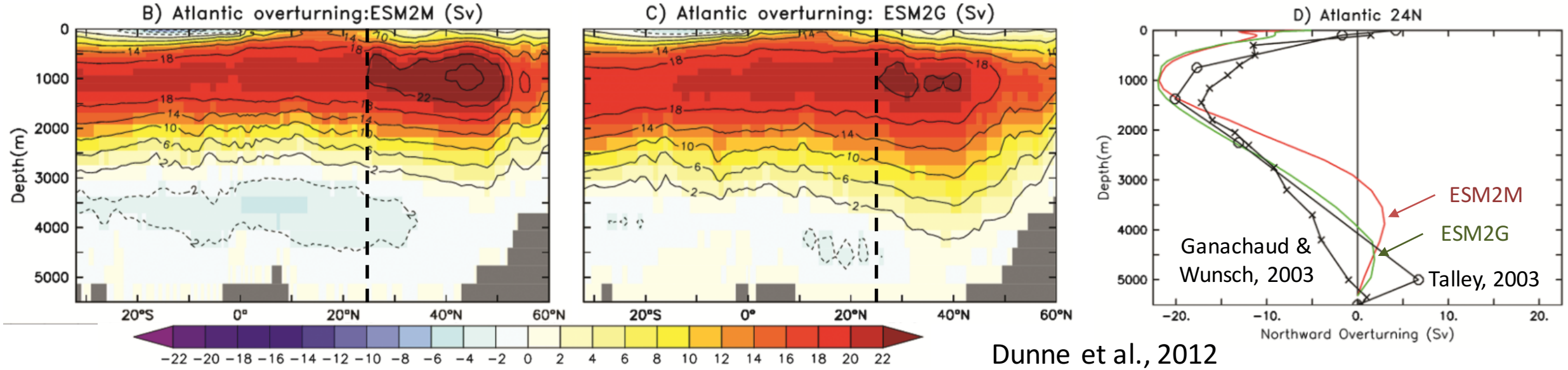

Dunne et al., 2012

Role of mesoscale eddies

- Delworth et al., 2012, coupled model series (CM2.1, CM2.5, CM2.6):
  - 50 km atmosphere
  - 1°, ¼° and 0.1° ocean
  - 1° alone has SGS eddy parameterization (Gent-McWilliams)
- Griffies et al., 2015, diagnosed how transient eddies in a 0.1° ocean transport heat upwards
  - CM2.6 least heat uptake of CM2.x series
  - Argue that CM2.5 has most heat uptake due to weak eddies and no GM

Evolution of horizontally averaged potential temperature, θ (°C).

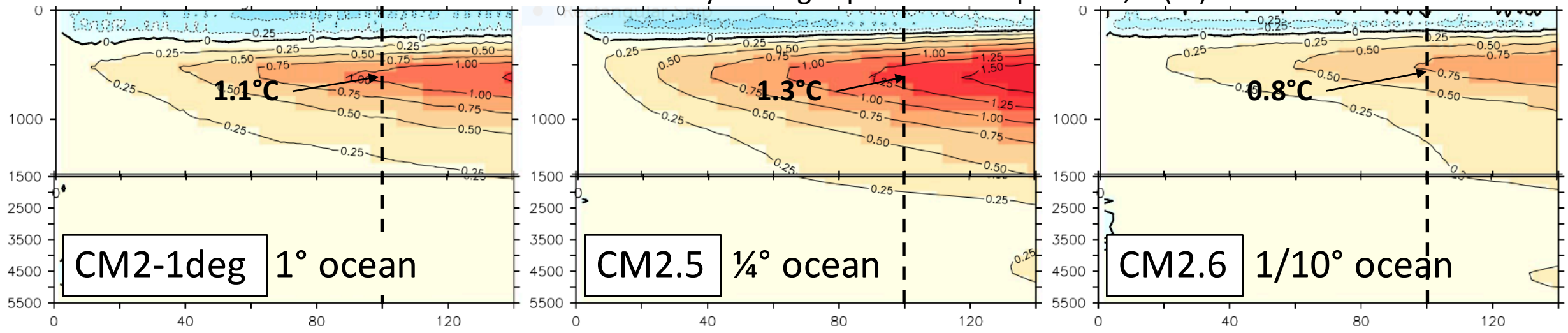

Measuring spurious mixing

- Measure work done by mixing in spin down experiments
  - Turning off explicit mixing leaves only numerical mixing*

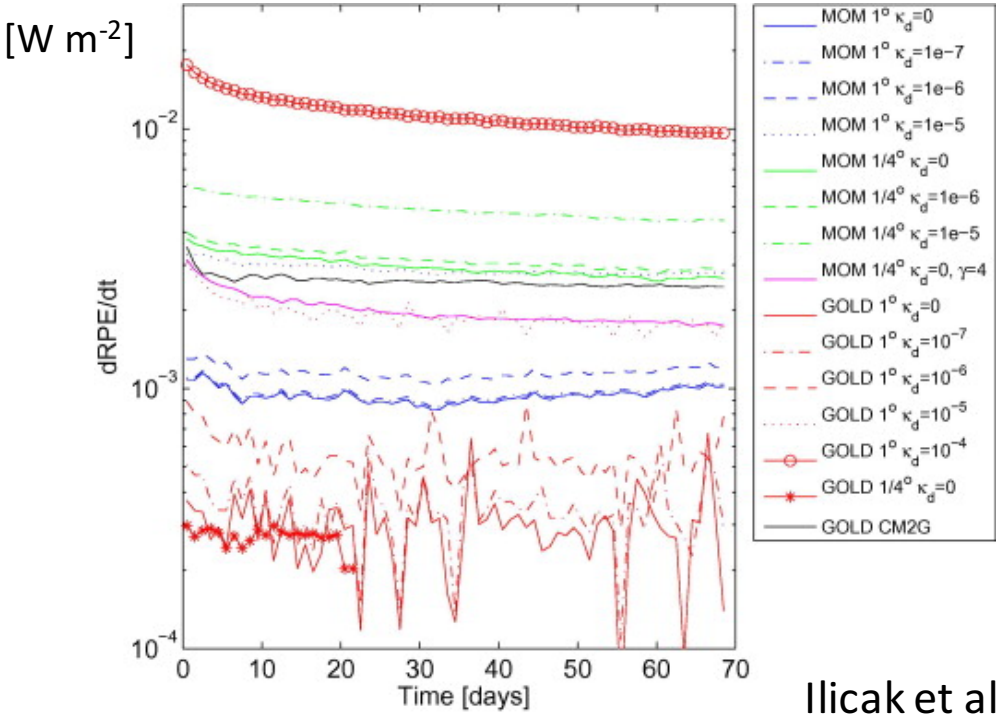

Ilicak et al., 2012

- Ilicak et al., 2012, argued ¼° z-coordinate model had numerical mixing as large as "real" mixing

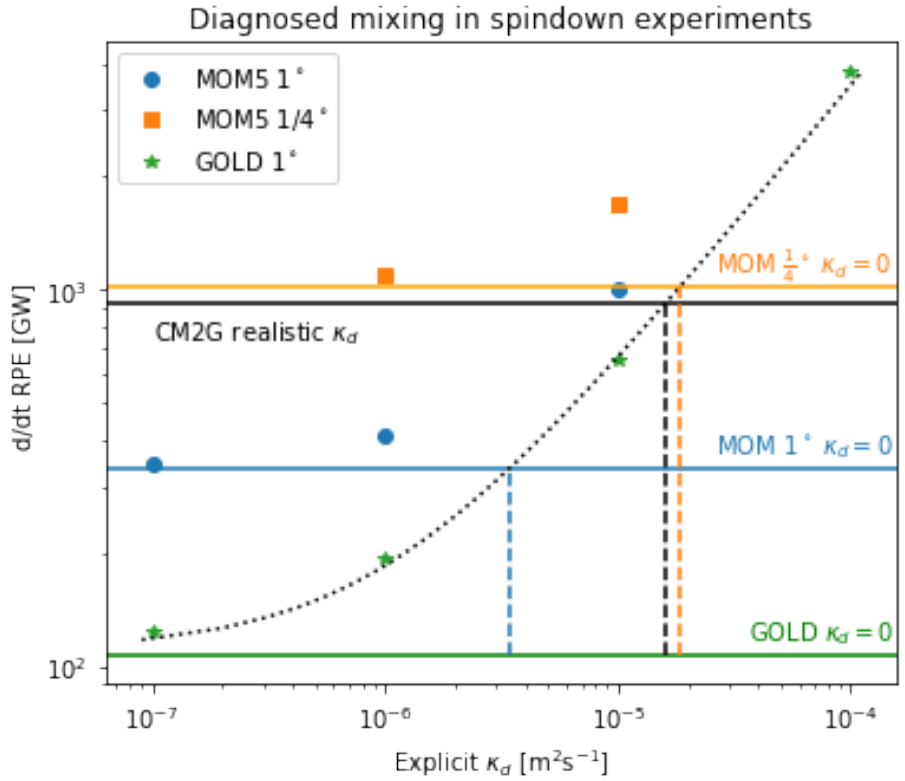

MOM6 and OM4

- Reducing spurious mixing motivated MOM6 development
  - General coordinate to avoid limitations of potential density (used by isopycnal layer models)
- MOM6 broadly reproduced prior solutions using z-coordinates
- Adoption of hybrid z-density coordinates reduced heat uptake
  - success?

Adcroft et al., 2019

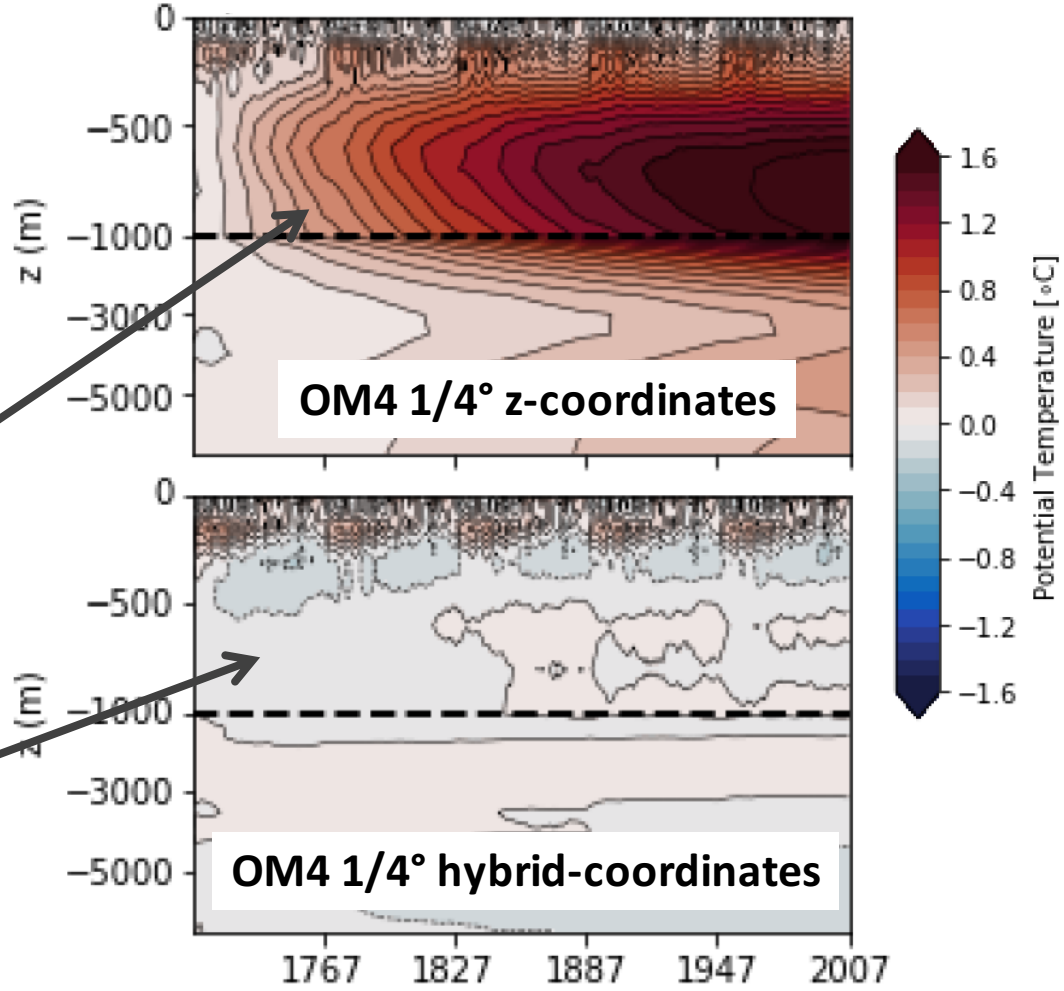

General coordinates (Boussinesq)

- Hydrostatic Primitive Equations (for ocean) in general coordinates $r = r(x, y, z, t)$:

$$\rho_0 \left(\frac{\partial \mathbf{u}}{\partial t} + (f + \zeta)\, \hat{\mathbf{z}} \wedge \mathbf{u} + \dot{r}\, \frac{\partial \mathbf{u}}{\partial r} + \nabla_r K \right) = -\nabla_r p - \rho \nabla_r \Phi + \mathcal{F}$$

$$\rho \frac{\partial \Phi}{\partial r} + \frac{\partial p}{\partial r} = 0$$

$$\frac{\partial z_r}{\partial t} + \nabla_r \cdot (z_r\, \mathbf{u}) + \frac{\partial (z_r\, \dot{r})}{\partial r} = 0 \qquad z_r = \frac{\partial z}{\partial r}$$

$$\frac{\partial (\theta\, z_r)}{\partial t} + \nabla_r \cdot (\theta z_r\, \mathbf{u}) + \frac{\partial (\theta\, z_r\, \dot{r})}{\partial r} = z_r \mathcal{N}_\theta^\gamma - \frac{\partial J_\theta^{(z)}}{\partial r}$$

$$\frac{\partial (S\, z_r)}{\partial t} + \nabla_r \cdot (S\, z_r\, \mathbf{u}) + \frac{\partial (S\, z_r\, \dot{r})}{\partial r} = z_r \mathcal{N}_S^\gamma - \frac{\partial J_S^{(z)}}{\partial r}$$

$$\rho = \rho\,(S, \theta, -g \rho_0 z(r))$$

Starr, 1945;
Kasahara, 1974; …

Layer integrated general coordinate equations

- Integrating between surfaces of constant r converts $z_r \rightarrow h = \int z_r dr$ and $\partial_r \rightarrow \delta_r$

$$\rho_0 \left(\frac{\partial \mathbf{u}}{\partial t} + \frac{(f+\zeta)}{h} \hat{\mathbf{z}} \wedge h\,\mathbf{u} + \dot{r} \frac{\partial \mathbf{u}}{\partial r} + \nabla_r K \right) = -\nabla_r p - \rho \nabla_r \Phi + \mathcal{F}$$

$$\rho\, \delta_r \Phi + \delta_r p = 0$$

$$\frac{\partial h}{\partial t} + \nabla_r \cdot (h\,\mathbf{u}) + \delta_r (z_r \dot{r}) = 0$$

$$\frac{\partial (\theta\, h)}{\partial t} + \nabla_r \cdot (\theta h\,\mathbf{u}) + \delta_r (\theta\, z_r \dot{r}) = h \mathcal{N}_\theta^\gamma - \delta_r J_\theta^{(z)}$$

$$\frac{\partial (S\, h)}{\partial t} + \nabla_r \cdot (S\, h\,\mathbf{u}) + \delta_r (S\, z_r \dot{r}) = h \mathcal{N}_S^\gamma - \delta_r J_S^{(z)}$$

$$\rho = \rho\,(S, \theta, -g \rho_0 z(r))$$

- Choosing $\dot{r} = 0$ follows the vertical motion → Vertically Lagrangian
  - removes explicit vertical transports → no vertical CFL

Lagrangian remap algorithm

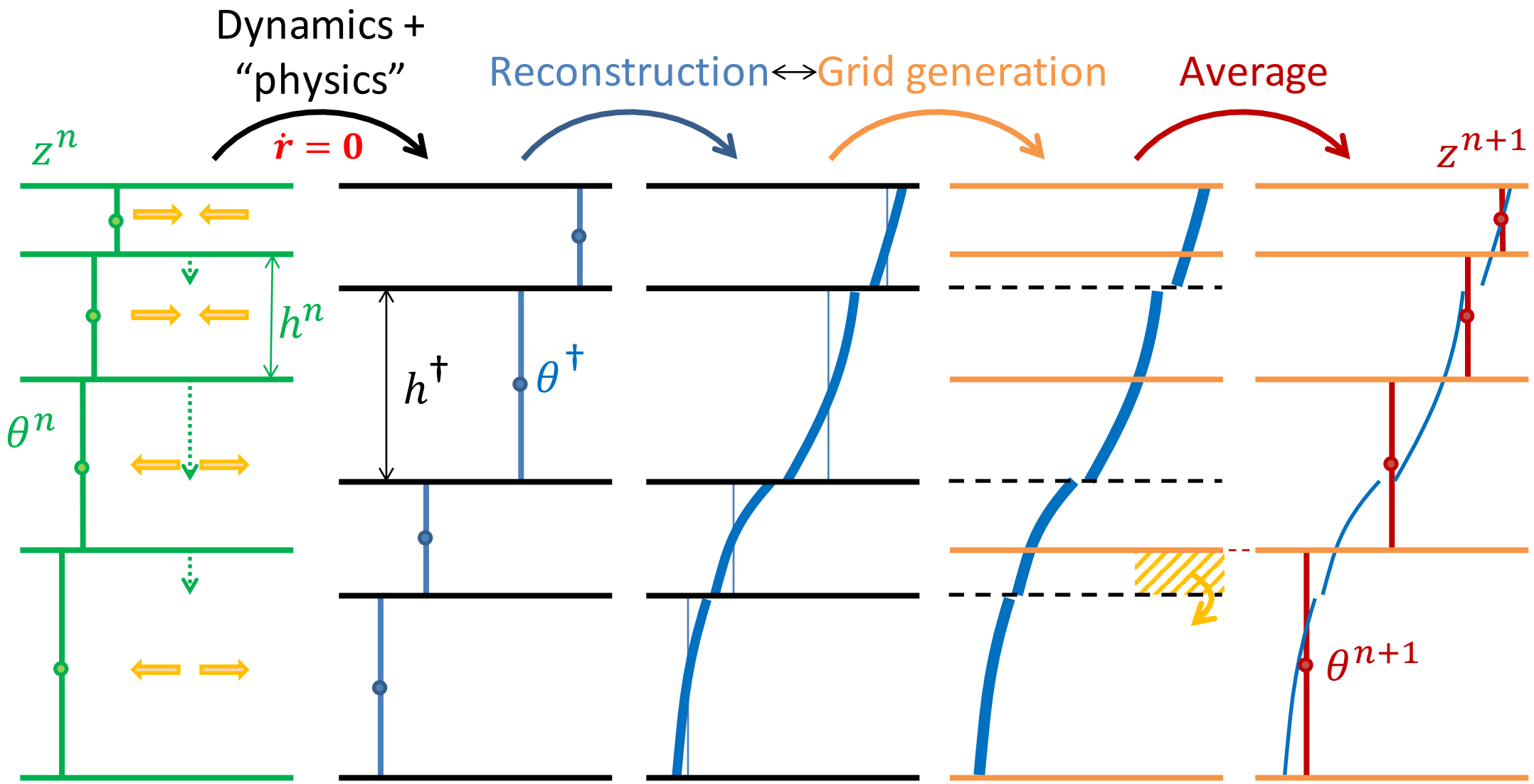

Eulerian, ALE and LRM algorithms side-by-side

Eulerian

$$\partial_z p = -g\rho(z, S^n, \theta^n)$$

$$v_h^{n+1} = v_h^n + \Delta t\left(-\frac{1}{\rho_o}\nabla_z p + \cdots\right)$$

$$\partial_z w = -\nabla \cdot v_h^{n+1}$$

$$\theta^{n+1} = \theta^n - \Delta t\left[\begin{matrix}\nabla \cdot \left(v_h^{n+1}\theta^n\right) + \\ \partial_z(w\theta^n) + \cdots\end{matrix}\right]$$

Assuming explicit-in-time transport

$$\frac{w\Delta t}{\Delta z} < 1$$

A.L.E.

introduces grid motion w_g

$$\partial_z p = -g\rho(z, S^n, \theta^n)$$

$$v_h^{n+1} = v_h^n + \Delta t\left(-\frac{1}{\rho_o}\nabla_z p + \cdots\right)$$

$$\delta_k(w^* + w_g) = -\nabla \cdot h^n v_h^{n+1}$$

$$h^{n+1} = h^n + \Delta t\,\delta_k(w_g)$$

$$h^{n+1}\theta^{n+1} = h^n\theta^n - \Delta t\left[\begin{matrix}\nabla \cdot \left(h^n v_h^{n+1}\theta^n\right) \\ +\delta_k(w^*\theta^n) + \cdots\end{matrix}\right]$$

Assuming explicit-in-time transport

$$\frac{w^*\Delta t}{\Delta z} < 1$$

$$w^* = w - w_g$$

Langrangian-remap

$$\partial_z p = -g\rho(z, S^n, \theta^n)$$

$$v_h^\dagger = v_h^n + \Delta t\left(-\frac{1}{\rho_o}\nabla_z p + \cdots\right)$$

$$h^\dagger = h^n - \Delta t\nabla \cdot (h^n v_h^\dagger)$$

$$h^\dagger\theta^\dagger = h^n\theta^n - \Delta t\left[\nabla \cdot \left(\begin{matrix}h^n v_h^\dagger\theta^n \\ + \cdots\end{matrix}\right)\right]$$

$$h^{n+1} \leftarrow \delta_k Z\left(z^\dagger\right)$$ *Grid generation*

$$\theta^{n+1} = \theta^\dagger\left(Z(z^\dagger)\right)$$ *Remap*

Sub-cycling with Lagrangian vertical dynamics

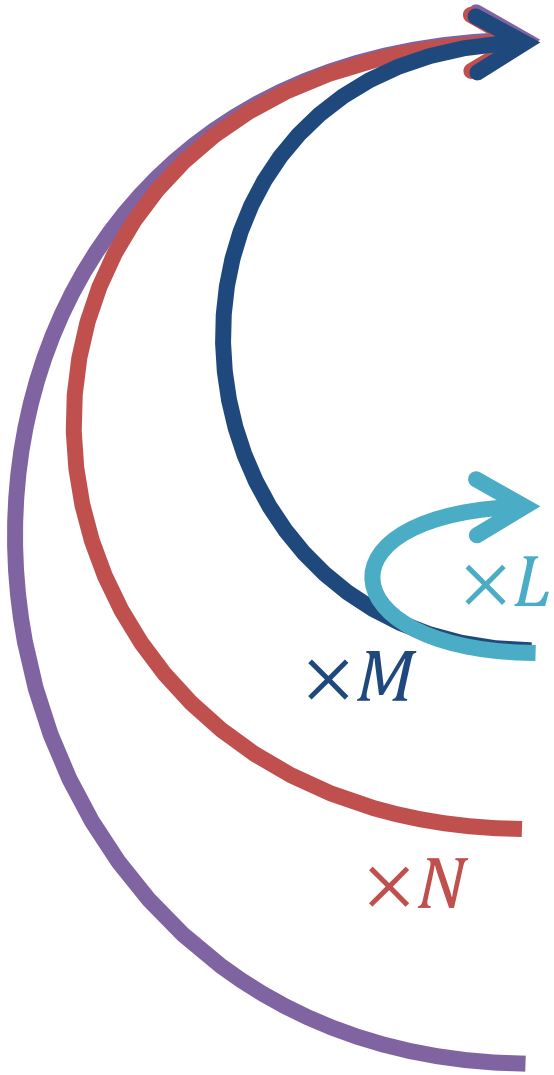

$$\delta_k p = -\rho(z, S^n, \theta^n)\delta_k \Phi$$

$$v_h^{m+1} = v_h^m + \frac{1}{M}\frac{\Delta t}{\rho_o}(-\nabla_r p - \rho \nabla_r \Phi + \cdots)$$

$$h^{m+1} = h^m - \frac{1}{M}\Delta t \nabla_r \cdot (h^m v_h^{m+1})$$

Internal gravity waves

$$\frac{\Delta t c_{ig}}{\Delta x} < 1$$

$$U^{l+1} = U^l + \frac{1}{L}\Delta t(-\nabla \eta^l + \cdots)$$

$$\eta^{l+1} = \eta^m - \frac{1}{L}\Delta t \nabla_r \cdot (H U^{l+1})$$

Barotropic gravity waves

$$\frac{\Delta t \sqrt{gH}}{L \Delta x} < 1$$

$$h^* C^* = h^n C^n - M\Delta t \left[\nabla \cdot \left(\sum_{m=1}^{M} h^m v_h^{m+1} C^n\right)\right]$$

Tracers

$$\frac{M \Delta t u_h}{\Delta x} < 1$$

$$h^{n+1} \leftarrow \delta_k Z(h^*)\,; C^{n+1} = C^*(Z(h^*))\,; \ldots$$

Vertical remap

Consistent grid-generation and remapping

Interpolation for grid generation

- Accurate
- **Continuous** (single valued)
  - resulting profiles are generally not conservative

Reconstruction for remapping

- Accurate
- **Conservative**
  - profiles often become discontinuous to be conservative

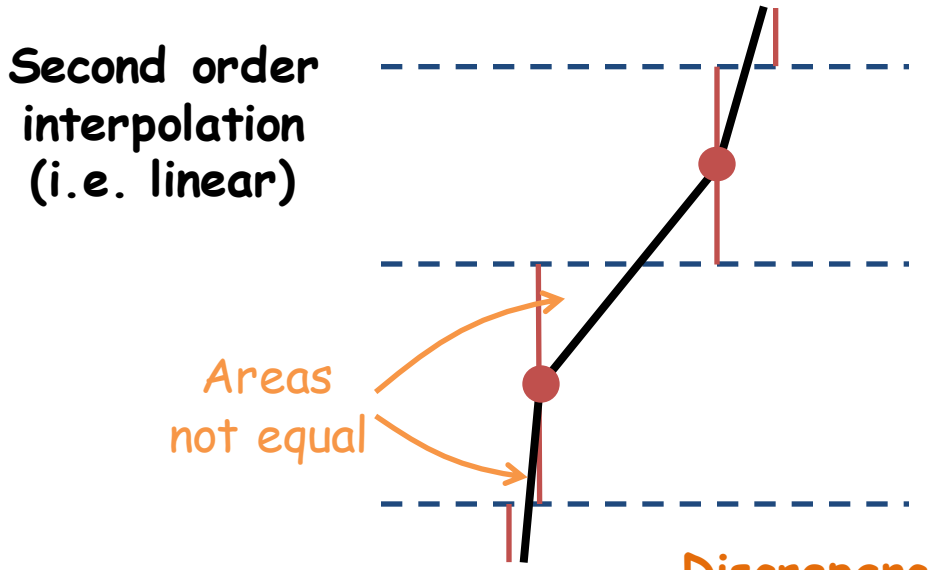

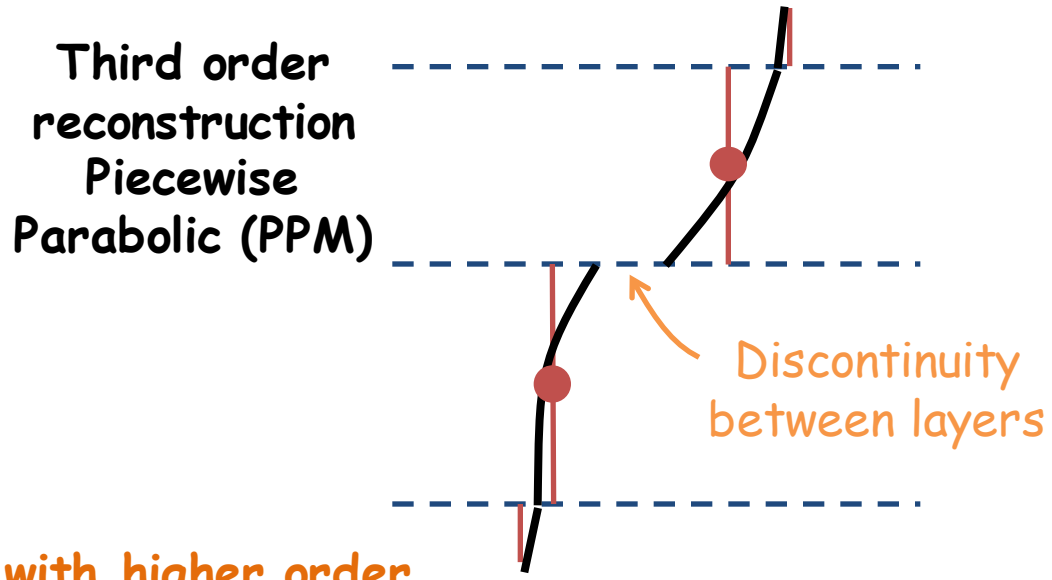

Discrepancies reduce with higher order

Remapping implementations

Remapping via "advective flux"

$$h_k^{n+1}\theta_k^{n+1} = h_k^{\dagger}\theta_k^{\dagger} + \left(\int_{z^{\dagger}_{k+\frac{1}{2}}}^{z^{n+1}_{k+\frac{1}{2}}} \theta^{\dagger} dz - \int_{z^{\dagger}_{k-\frac{1}{2}}}^{z^{n+1}_{k-\frac{1}{2}}} \theta^{\dagger} dz \right)$$

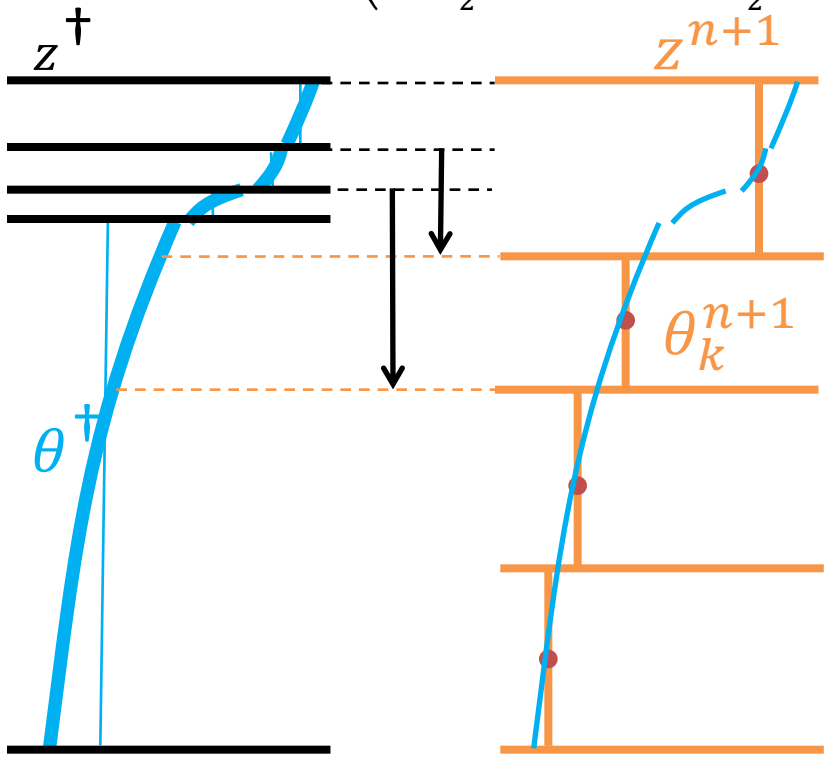

Accurate conservation but locally inaccurate **for CFL>1**

Remapping by "projection"

$$h_k^{n+1}\theta_k^{n+1} = \int_{z^{n+1}_{k+\frac{1}{2}}}^{z^{n+1}_{k-\frac{1}{2}}} \theta^{\dagger} dz$$

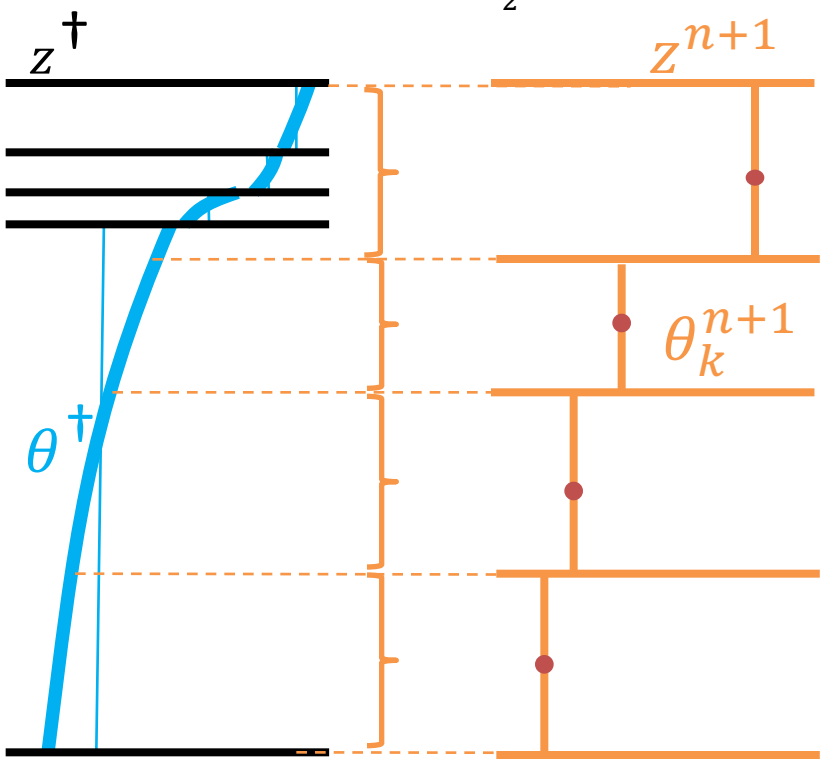

Inaccurate total conservation but accurate locally

Accurate conservation when remapping

Remap by “sub layers”

- Divide superset of old/new grids into sub layers (2N-1)
- Integrate profile for each sub-layer
  - By definition uses only one source layer profile
- Replace *largest* sub-layer with

$$h_j^s \theta_j^s = h_k^\dagger \theta_k^\dagger - \sum_{j'=l}^{m} (1 - \delta_{j'j}) h_{j'}^s \theta_{j'}^s$$

(insight from Hallberg)

- Sum sub-layers to new layer

$$h_j^s \theta_j^s = \int_{z^s_{j+\frac{1}{2}}}^{z^s_{j-\frac{1}{2}}} \theta^\dagger dz \qquad h_k^{n+1} \theta_k^{n+1} = \sum_{j=l}^{m} h_j^s \theta_j^s$$

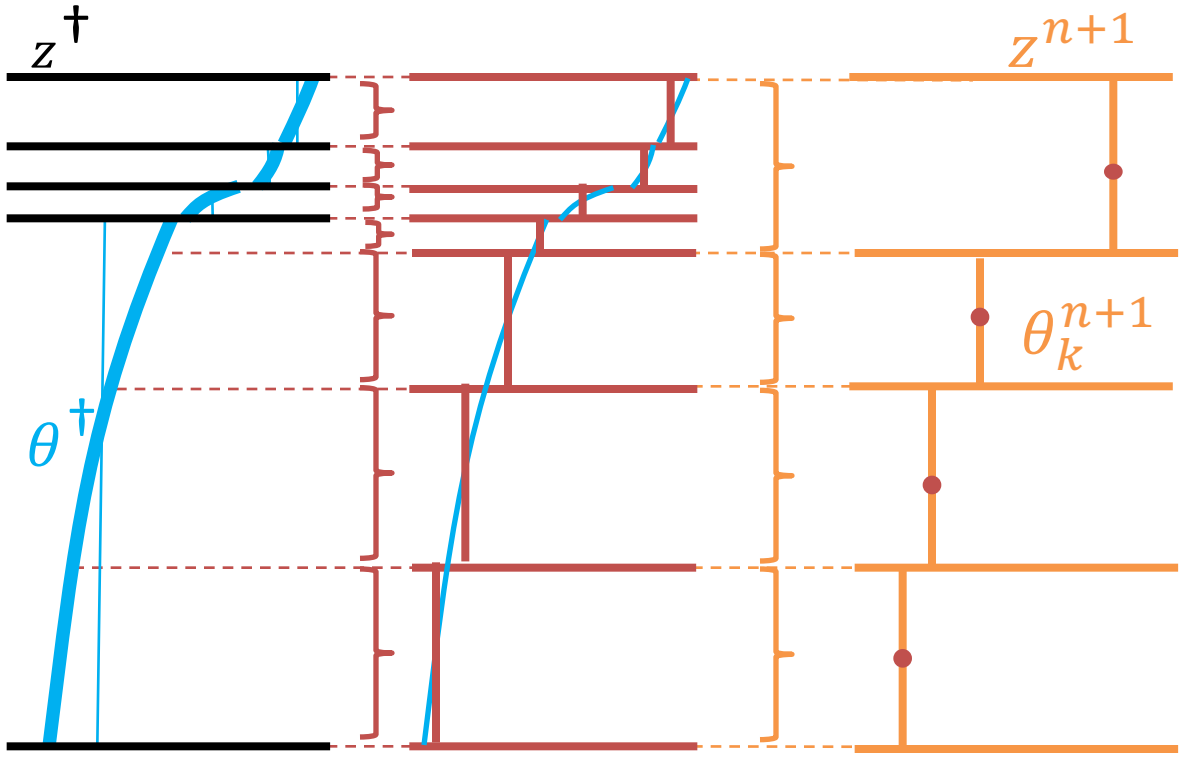

Piecewise * Methods (* = C,L,P or Q)

- PLM: two degrees of freedom
  - Cell mean + slope
- PPM: three degrees of freedom
  - Very widely used
  - Cell mean + two edge values
- PQM: five degrees of freedom
  - Cell mean + two edge values + two edge slopes (White & Adcroft, JCP 2008)

Inspired by Daru & Tenaud, JCP 2004 – introduced OS_i i=1..7

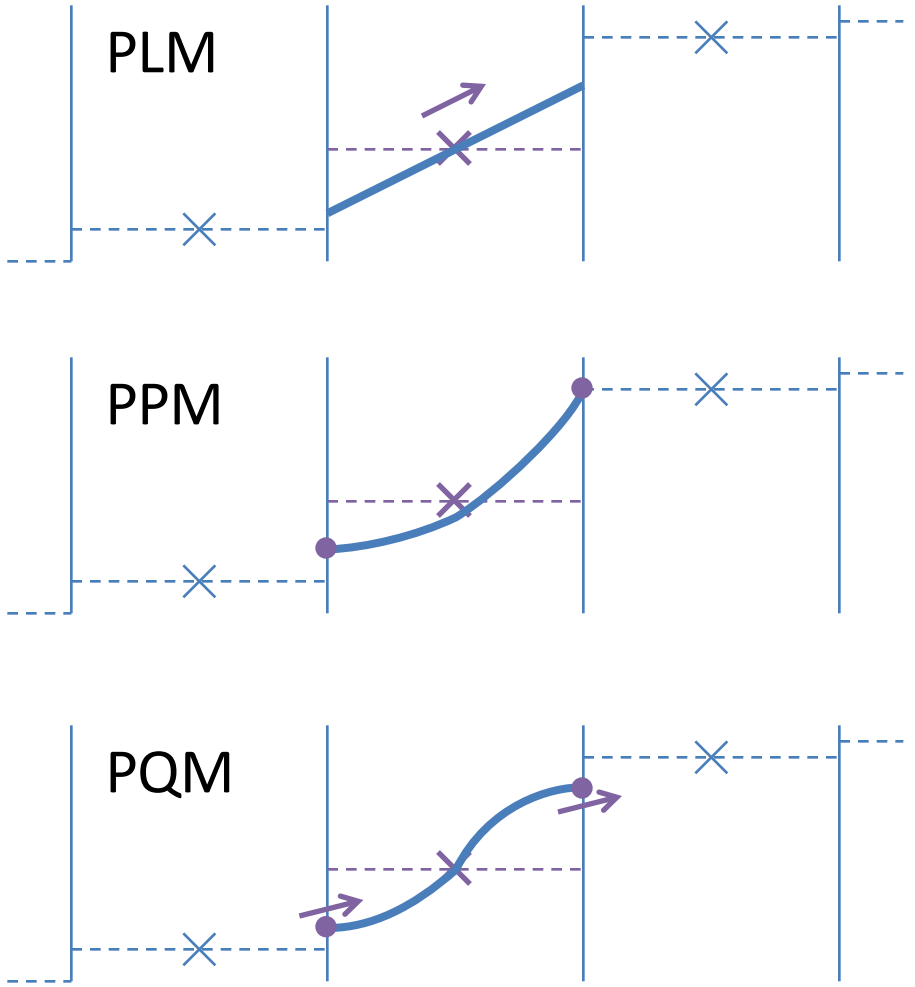

Successive schemes provide more flexibility to represent structures → more accurate

Illustrating methods and spurious diffusion

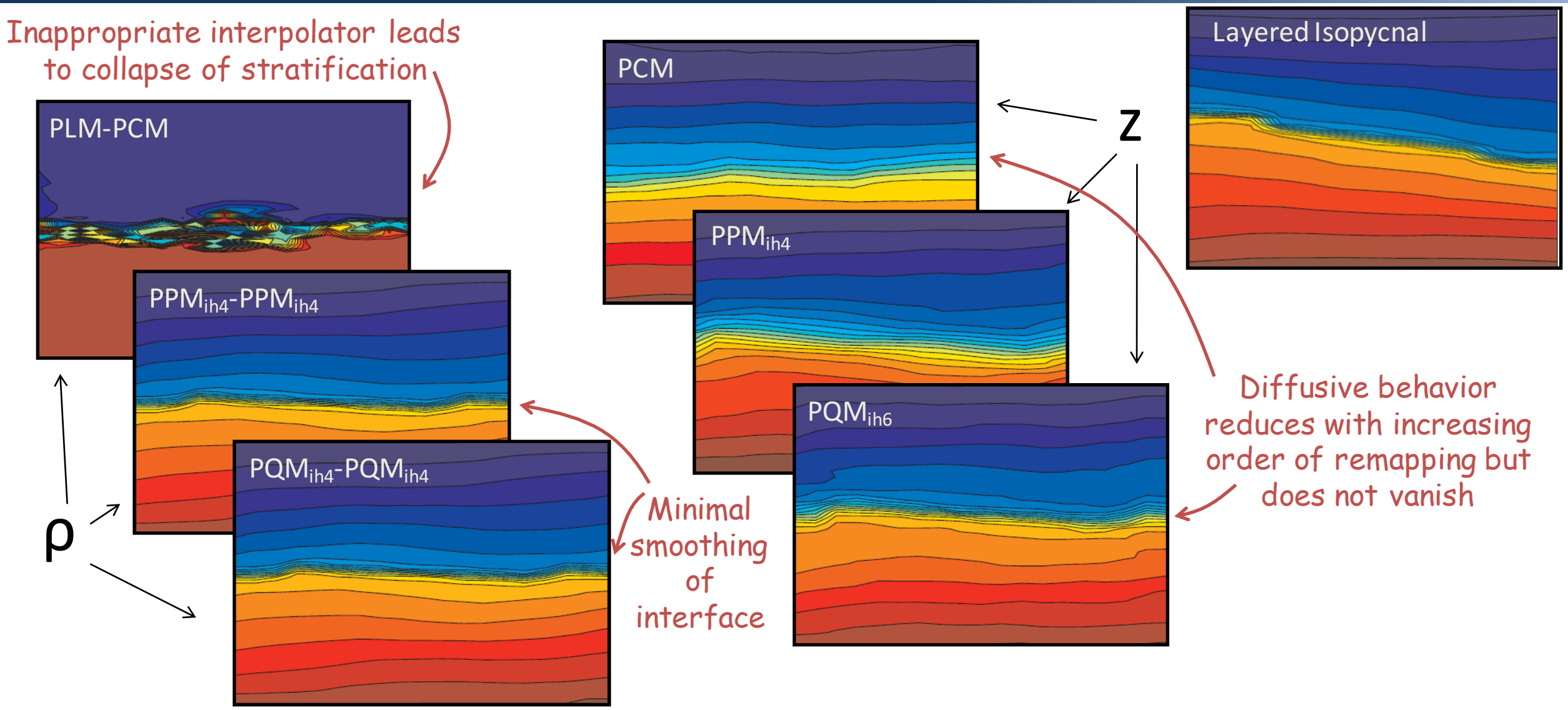

Overflows

- Dense flow down a slope
  - Hydrostatic and adiabatic
- Layered isopycnal solution is truly adiabatic
- z* and terrain-following both have modified water masses
- LRM + density coordinates (found by interpolation) behaves very similarly to layered model

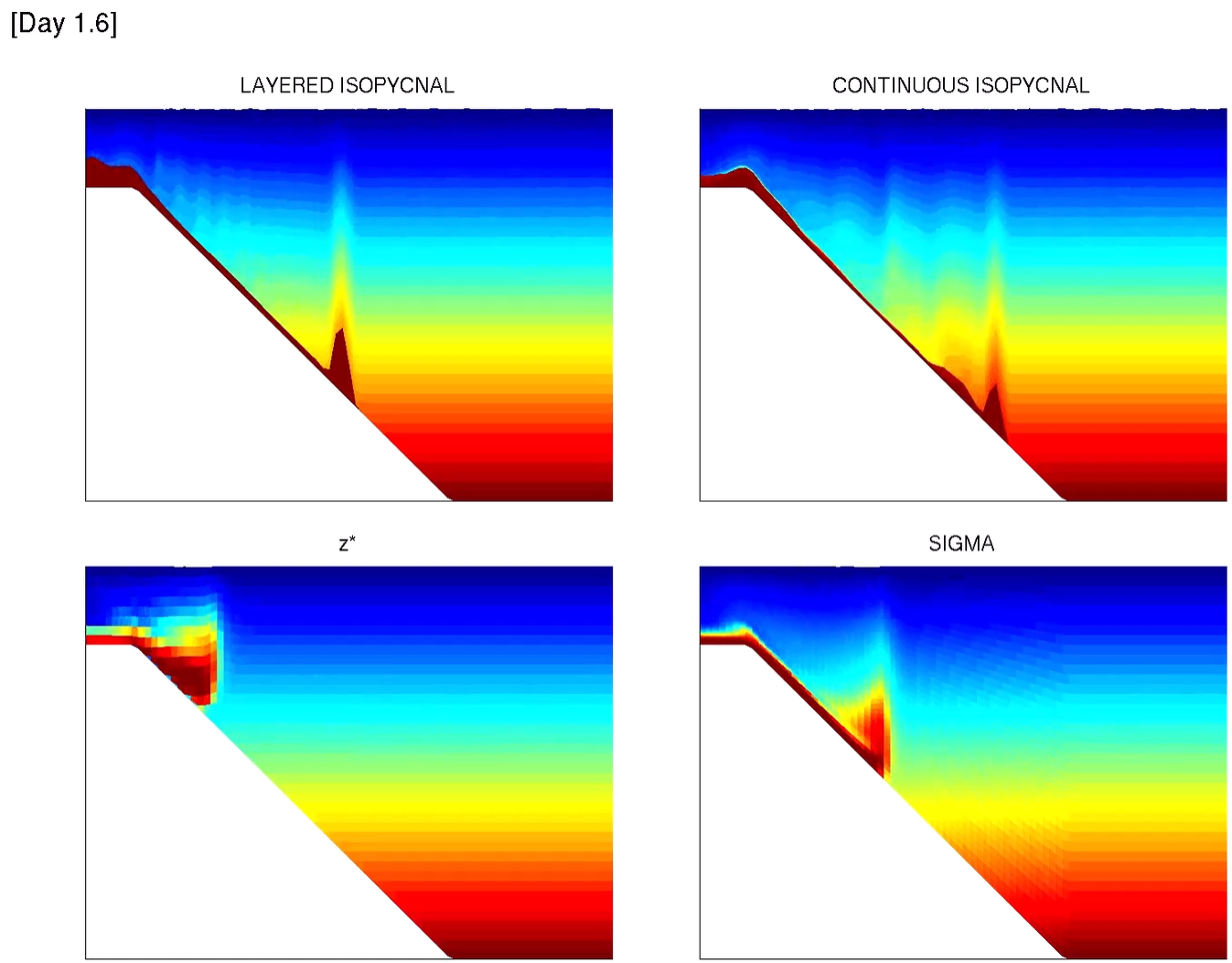

Sources of spurious mixing

- Lateral processes (incl. transport) acting on inclined isopycnals

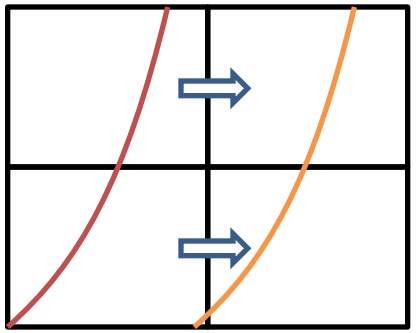

- Along isopycnal processes in non-isopycnal coordinates

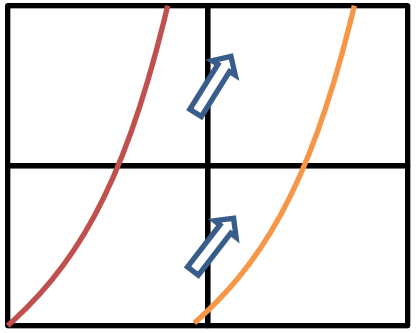

- Dia-surface transport in vertical
  - Minimizing dia-surface motion reduces numerical diffusion

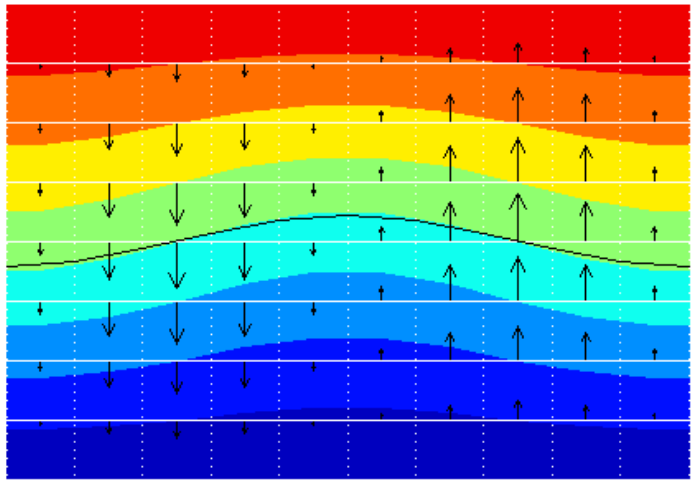

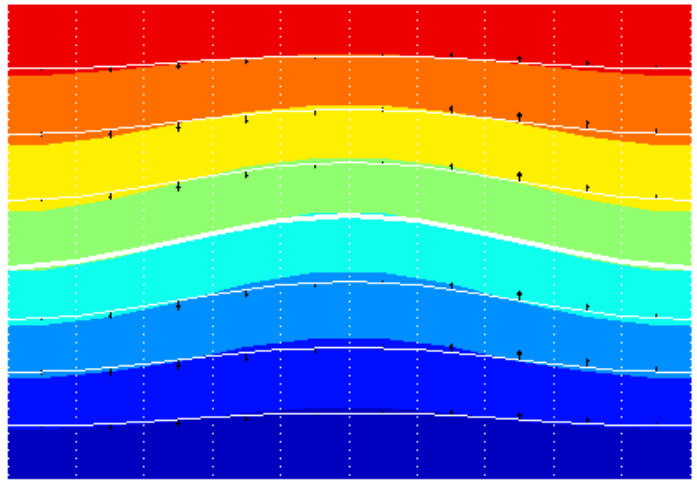

- Choosing a coordinate close to isopycnal is desirable to minimize spurious diffusion

Hybrid and other coordinates

- Already know that pure isopycnal coordinates have limitations
- Bleck, 2002, introduced hybrid z-rho coordinate in HYCOM

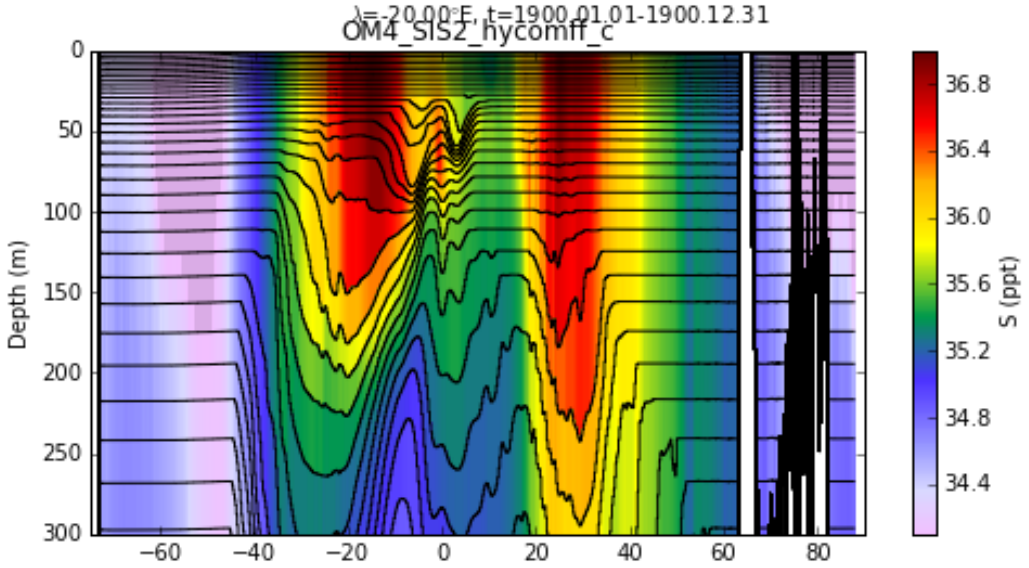

- z-tilde: Leclair & Madec, 2011; Petersen et al., 2015
- adaptive: Hofmeister et al., 2010; Gräwe et al., 2015; Gibson (thesis) 2019

- OM4 used “HYCOM1” which is a simple interpretation of actual HYCOM hybrid coordinate
  - Ongoing work with Wallcraft and Chassignet to improve grid generation (c.f. AMOC results)

Balancing heat transfer by eddies and mixing

- Comparing z* to hybrid coordinate provides magnitude of spurious numerical mixing
- Reducing resolution from ¼° to ½° (eddying to non-eddying) inhibits resolved re-stratification
  - ½° requires eddy parameterization
- Refining resolution from ¼° to ⅛° reduces heat uptake:
  - more efficient eddies
  - and/or less numerical mixing?

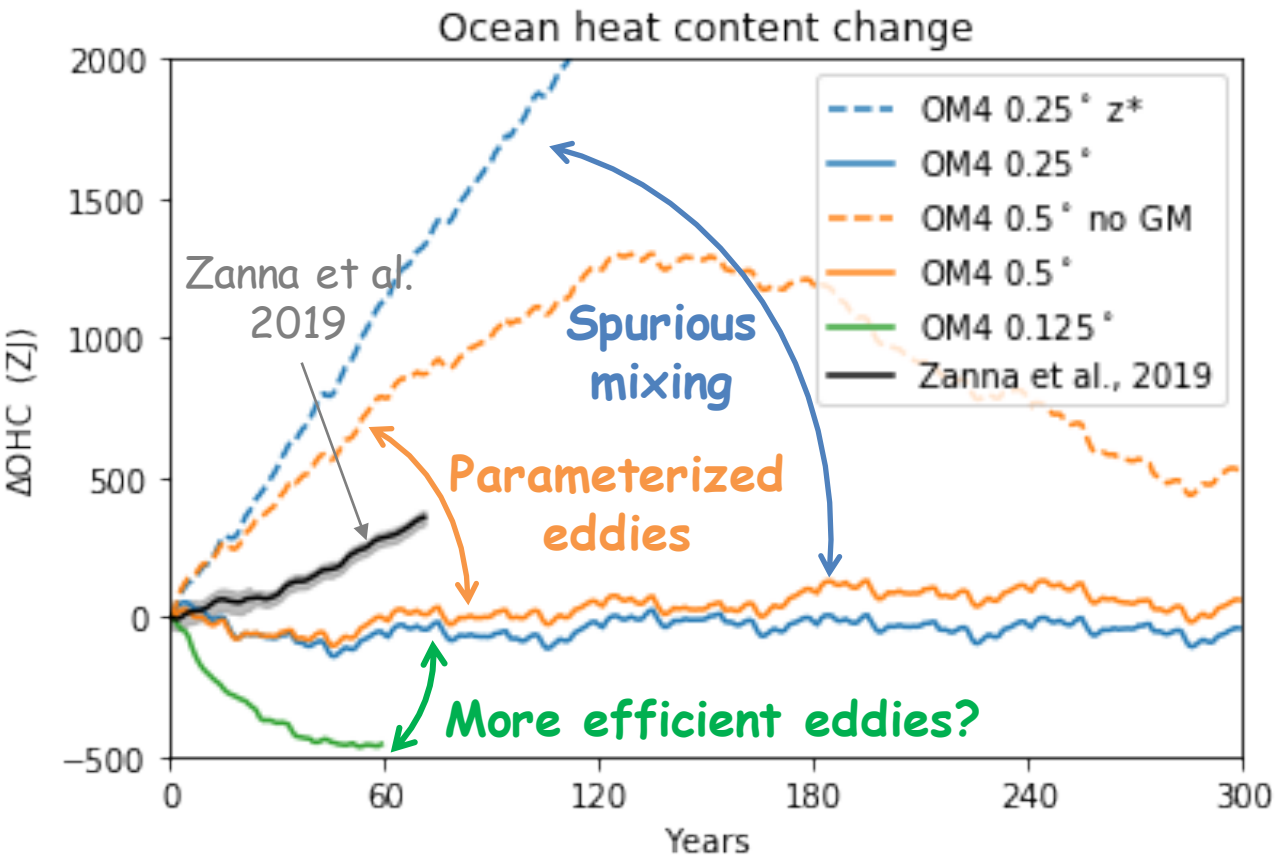

- This really tells us we (inadvertently) managed to perfectly compensate for weak eddies at ¼° resolution

OM4 AMOC

- Main concern is OM4 with hybrid coordinate still has a shallow AMOC
  - Is this mixing in overflows?

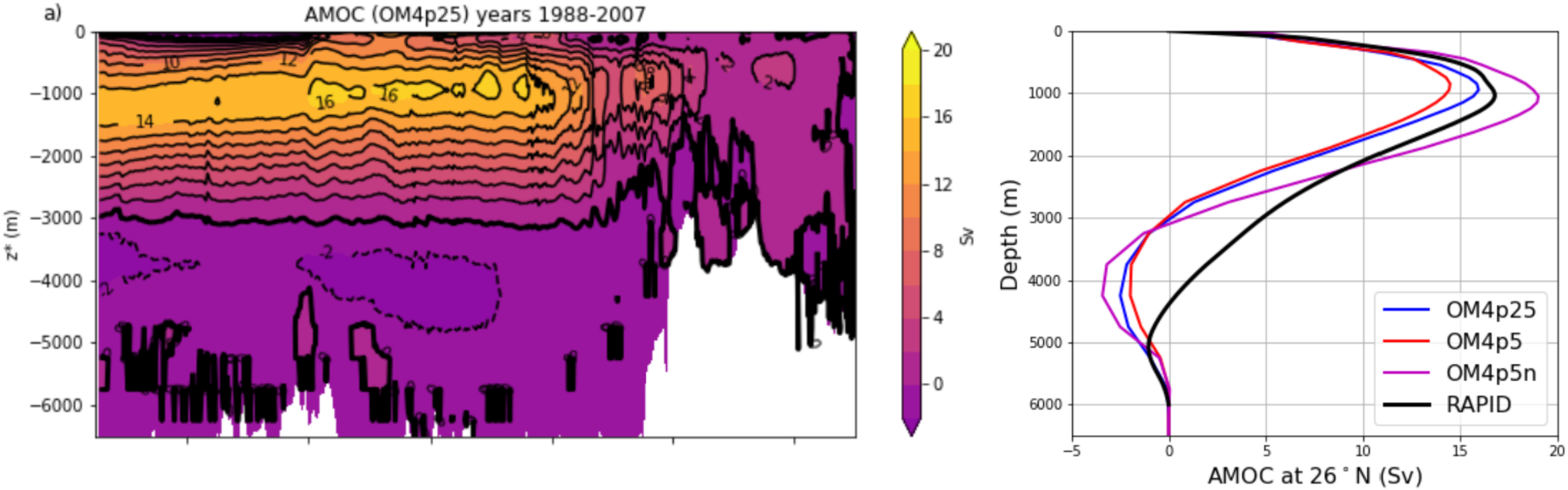

  - It turns out we did have too much parameterized mixing but reducing that has had no affect on depth of AMOC. In fact nothing we've tried so far seems to!

Wrap up

- Motivated by results with isopycnal layered models we built MOM6, capable of using arbitrarily general coordinates following HYCOM's pioneering hybrid coordinate
- Lagrangian Remap Algorithm has significant advantages for Earth System Models with many constituents
- High-order numerical methods + LRM deliver low levels of spurious mixing
- In OM4, putting everything together, a mystery remains as to why AMOC is shallower than in ESM2G

Quantifying spurious mixing using energetics

- Potential energy

$$\mathrm{PE} = g \iiint \rho z \, dV$$

- Available potential energy (APE)

$$\mathrm{APE} = \mathrm{PE} - \mathrm{RPE}$$

$$\mathrm{RPE} = g \iiint \rho^* z \, dV$$

- ρ* is the adiabatically re-arranged state with minimal potential energy
- **RPE can only be changed by diapycnal mixing**
  - Mixing raises center of mass

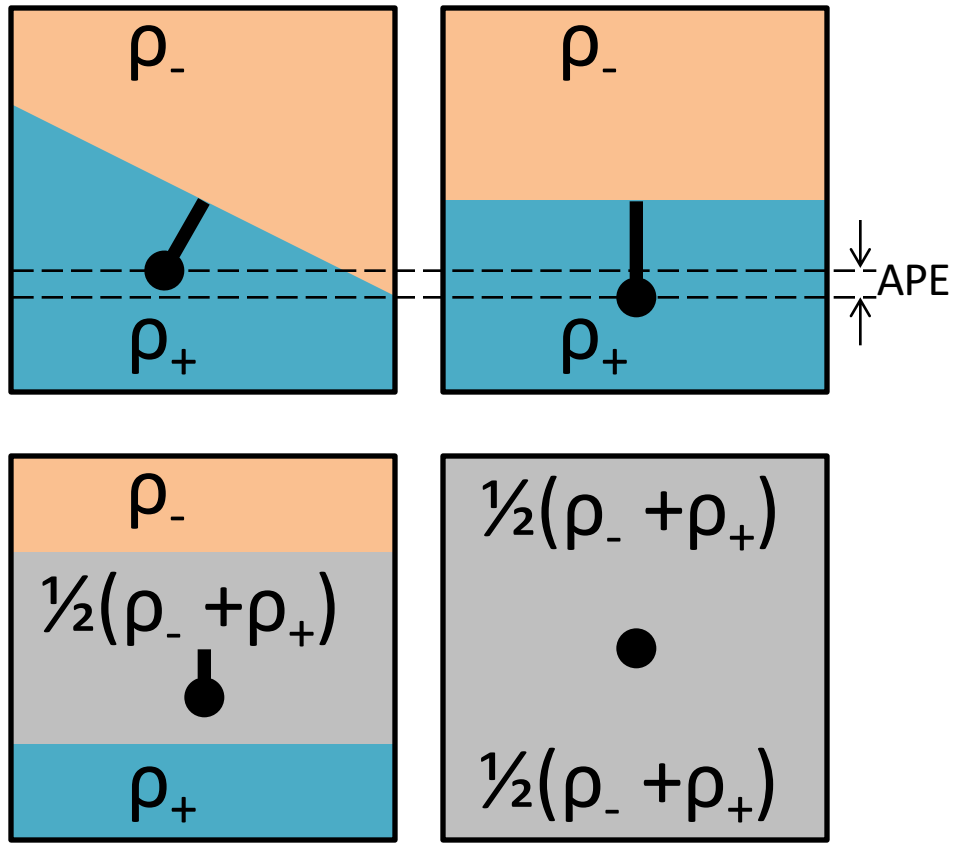

Winters et al., JFM 1995
Ilicak et al., OM 2012

OM4

- OM4 is the ice-ocean component of GFDL's latest coupled model CM4 (Held et al., 2019)
- OM4 configuration
  - Identical setup/parameters to CM4
  - Developed almost exclusively in coupled mode
    - Uncoupled OM4
  - Nominally eddy-permitting ¼° horizontal resolution
    - Non-eddying ½° with eddy parameterization (GM+EKE scheme)

Ingredients:

- MOM6
  - using hybrid z-ρ vertical coordinates
    c.f. HYCOM, Bleck 2002
- ePBL
  - Reichl and Hallberg, 2019
- Scale-aware MLE restratification
  - Fox-Kemper et al., 2011
- Shear-dependent mixing
  - Jackson et al., 2008
- Internal-wave driven mixing
  - Melet et al., 2012
- BBL
  - Legg et al., 2006

Adcroft et al., *JAMES* 2019